

NLTE models of line-driven stellar winds

III. Influence of X-ray radiation on wind structure of O stars

Jiří Krtička^{1*} and Jiří Kubát^{2*}

¹Ústav teoretické fyziky a astrofyziky, Masarykova univerzita, CZ-611 37 Brno, Czech Republic

²Astronomický ústav AV ČR, Fričova 298, CZ-251 65 Ondřejov, Czech Republic

Received

ABSTRACT

We study the influence of X-rays on the wind structure of selected O stars. For this purpose we use our non-local thermodynamic equilibrium (NLTE) wind code with inclusion of additional artificial source of X-rays, assumed to originate in the wind shocks.

We show that the influence of shock X-ray emission on wind mass-loss rate is relatively small. Wind terminal velocity may be slightly influenced by the presence of strong X-ray sources, especially for stars cooler than $T_{\text{eff}} \lesssim 35\,000$ K.

We discuss the origin of the $L_X/L \sim 10^{-7}$ relation. For stars with thick wind this relation can be explained assuming that the cooling time depends on wind density. Stars with optically thin winds exhibiting the “weak wind problem” display enhanced X-ray emission which may be connected with large shock cooling length. We propose that this effect can explain the “weak wind problem”.

Inclusion of X-rays leads to a better agreement of the model ionization structure with observations. However, we do not find any significant influence of X-rays on P V ionization fraction implying that the presence of X-rays cannot explain the P V problem.

We study the implications of modified ionization equilibrium due to shock emission on the line transfer in the X-ray region. We conclude that the X-ray line profiles of helium-like ions may be affected by the line absorption within the cool wind.

Key words: stars: winds, outflows – stars: mass-loss – stars: early-type – hydrodynamics – X-rays: stars

1 INTRODUCTION

The evolution of hot stars seems to be strongly influenced by the loss of a substantial part of their mass via winds. Consequently, a proper knowledge of amount of material expelled from the stellar surface per unit of time (mass loss rate) is necessary for the stellar evolution calculations.

There exist some serious problems with mass-loss rate predictions for hot stars. The situation is not satisfactory even in the O star domain, where several different theoretical models are available (e.g., Vink et al. 2000, Pauldrach et al. 2001, Puls et al. 2003, Krtička & Kubát 2004, hereafter Paper I). A good agreement between these theoretical models and observations may be just illusory effect of the possible manifestation of local wind inhomogeneities (clumping) in the observed spectra (e.g., Bouret et al. 2003, Martins et al. 2005, Puls et al. 2006b). The problem is that the spectrum of a clumped wind with small mass-loss rate may mimic the spectrum of a smooth wind with large mass-loss rate. Consequently, the mass-loss rates derived from observations with account of clumping may be significantly lower than those derived

without taking into account the influence of clumping. Lower mass-loss rates are indicated also by weak P V wind lines (Fullerton et al. 2006), and by the study of X-ray line profiles (Owocki & Cohen 2006). If the mass-loss rates derived from observations are really much lower due to the influence of clumping on the observed spectra, then there exists a significant discrepancy between theory and observation (Puls et al. 2006a).

Moreover, some O stars with low luminosities exhibit the so-called “weak wind problem” (Bouret et al. 2003; Martins et al. 2004; 2005; Krtička 2006). Theoretically predicted mass-loss rates of these stars are much higher than the mass-loss rates inferred from observations (even without taking into account the clumping). The origin of this discrepancy is unclear.

One of the reasons that may cause these mentioned differences between observation and theory of hot star winds is the neglect of X-ray radiation. The X-ray radiation of hot stars is likely generated by the wind shocks that exist in the wind either due to the instability caused by the radiative driving (Owocki et al. 1988, Feldmeier et al. 1997b) or due to the collisions of wind streams channelled by the magnetic field (Babel & Montmerle 1997, ud-Doula & Owocki 2002). The X-rays may be generated also due to decoupling of wind components accompanied by frictional heating (Kubát et al. 2004).

* E-mail: krticka@physics.muni.cz (JKr); kubat@sunstel.asu.cas.cz (JKu)

In the case of binaries the X-rays may also originate in wind collisions (Prilutskii & Usov 1976; Antokhin et al. 2004).

X-ray radiation influences above all trace ionization states in most of hot O stars (MacFarlane et al. 1994) and the inclusion of X-ray sources is necessary especially for the correct prediction of hot star spectra (Pauldrach et al. 2001). On the other hand, for cooler stars the wind ionization balance may be dominated by the influence of X-ray radiation (MacFarlane et al. 1994).

Recently Fullerton et al. (2006) showed that the mass-loss rate determined from the P v lines is much lower than that derived from the H α line or radio emission. This implies also that hot star wind mass-loss rates determined from P v lines are significantly lower than the theoretical ones. However, this conclusion is sensitive to the ionisation state of phosphorus. If P v is not a dominant ion at any effective temperature studied by Fullerton et al. (2006, e.g., due to the presence of X-rays), then the discrepancy between theory and observation of OB star winds may not be so significant. Hence, the inclusion of X-ray ionization may also be important from this perspective.

Thus, we present here a study of the influence of the X-ray radiation on the wind properties of O stars.

2 NLTE WIND MODELS

The process of calculation of models used in this paper was described in Paper I, thus here we only summarise its basic features and describe improvements.

2.1 Basic model description

Our models assume spherically symmetric stationary stellar wind.

Excitation and ionization state of elements important for the radiative driving and for the correct calculation of the radiative field is derived from the statistical equilibrium (NLTE) equations.

The radiative transfer equation is artificially split (as in the Paper I) into two parts, namely the radiative transfer in continuum and the radiative transfer in lines. The solution of the radiative transfer in continuum is based on the Feautrier method in the spherical coordinates (Mihalas & Hummer 1974 or Kubát 1993) with inclusion of all free-free and bound-free transitions of model ions, however neglecting line transitions. The radiative transfer in lines is solved in the Sobolev approximation (e.g., Castor 1974) neglecting continuum opacity and line overlaps.

The radiative force (calculated in the Sobolev approximation after (I.25)¹ using data extracted in 2002 from the VALD database (Piskunov et al. 1995, Kupka et al. 1999)) and the radiative cooling/heating term (we use the electron thermal balance method, Kubát et al., 1999) are calculated using occupation numbers derived from statistical equilibrium equations. Finally, the continuity equation, equation of motion, and energy equation are solved and consistent wind velocity, density, and temperature structure are obtained using iteration procedure. For our calculations we use Asplund et al. (2005) solar abundance determinations.

The lowest wavelength considered in the models is 7.5 Å and the largest X-ray wavelength is defined as 100 Å.

2.2 Inclusion of shock X-ray radiation

The consistent inclusion of X-ray generation into NLTE wind models (using hydrodynamical simulations that are able to predict the shock properties, Feldmeier et al. 1997b) is likely beyond the possibilities of present computers. To make the problem more tractable, and since we are interested in the effect of already generated X-rays on the wind, not in the process of X-ray generation itself, we use a simpler approach after Pauldrach et al. (1994), i.e., we include X-rays into our stationary models in an artificial way using two free parameters introduced below.

We assume that a part of wind material is heated to a very high temperature T_X due to the shock. The shock temperature is given by the Rankine-Hugoniot shock condition

$$T_X = \frac{3m_H}{32k} \left[u_X^2 + \frac{14}{5} a_H^2 \left(1 - \frac{3}{14} \frac{a_H^2}{u_X^2} \right) \right], \quad (1)$$

where k is the Boltzmann constant, m_H is the hydrogen mass, a_H is the sound speed calculated assuming a completely ionised hydrogen plasma,

$$a_H = \sqrt{\frac{10}{3} \frac{kT_H}{m_H}}, \quad (2)$$

where T_H is the hydrogen temperature taken from stationary wind models, and u_X is the upstream shock velocity,

$$u_X = u_{\text{rel}} v_r, \quad (3)$$

where v_r is the radial velocity in the stellar rest frame and u_{rel} is a dimensionless free parameter influencing the hardness of X-rays. Instead of the linear dependence of u_X on the wind velocity it would be possible to employ different assumptions, e.g., constant u_X . However, the observed X-rays originate at larger radii where the wind velocity approaches the terminal one, consequently such dependence would not result in a very different results. Moreover, in the case of constant u_X it would be necessary to introduce additional free parameter corresponding to the radius at which X-rays start to be emitted. Without it we would obtain unrealistically strong X-ray source at the wind base as the wind density is the largest there.

We add the X-ray emissivity

$$\eta_X(\nu) = f_X (\xi \rho)^2 \Lambda_\nu(T_X) / (4\pi), \quad (4)$$

into the emission coefficient, where f_X is the second free parameter determining the amount of X-rays (also called the filling factor), $\Lambda_\nu(T_X)$ is calculated using the Raymond-Smith X-ray spectral code (Raymond & Smith 1977, Raymond 1988), and ξ relates the wind density ρ and the electron number density

$$\xi = \frac{1}{m_H} \frac{1 + 2y}{1 + 4y}, \quad (5)$$

where y is the helium number density relative to the hydrogen one (here we assume a fully ionised gas).

We used different values of f_X in our calculations. The free parameter $u_{\text{rel}} = 0.3$ in all presented calculations. This roughly gives the same X-ray temperature compared to the results of numerical simulations (e.g., Owocki et al. 1988, Feldmeier et al. 1997b, Runacres & Owocki 2002) and observations (e.g., Berghöfer et al. 1997; Miller et al. 2002; Sana et al. 2006).

2.3 Joint calculation of wind model

In our previous work we split the calculation of wind model to parts below and above the critical point, at which the mass-loss rate of

¹ The equations from the Paper I are denoted as I.x, where x is the equation number there.

our stationary wind models is determined (Castor, Abbott & Klein 1975). This effectively means that we neglected the influence of the region above the critical point onto the region below this point. This was justifiable in our previous models with negligible contribution of X-ray radiation, because the wind close the critical point is optically thick in the UV region and optically thin for other wavelengths (except lines). The splitting of wind solution may not be legitimate in the case where additional sources of X-rays are present, because the X-rays that predominantly originate in the wind above the critical point, may penetrate downwards and, consequently, influence the solution below this point.

Here we calculate the joint wind model below and above the critical point already during the procedure of mass-loss rate determination. To do so, we first calculate several global iteration steps (during which we search for the base density corresponding to the solution which smoothly passes through the critical point, see Paper I) for models in which we account only for the wind close to the stellar surface. As soon as the appropriate base density is roughly known (with a precision of about 30%), we add the solution above the critical point and perform several additional global iteration steps until the base density is known with sufficiently high precision of 1%. This approach enables us to properly take into account the influence of X-rays on the mass-loss rate.

2.4 Statistical equilibrium equations

The statistical equilibrium equation for level i of a given atom (ion) has the form (Mihalas 1978, also (I.1))

$$\sum_{j \neq i} N_j P_{ji} - N_i \sum_{j \neq i} P_{ij} = 0, \quad (6)$$

where N_i , N_j are relative occupation numbers of studied levels ($N_i = n_i/n_{\text{atom}}$, where n_i is the number density of atoms in given excitation and ionization state i and n_{atom} is the total number density of given atoms; similarly for the level j). P_{ij} are rates of all processes by which an atom can change its state (see e.g., Mihalas 1978). Note that for simplicity we do not explicitly write the radial dependence of all variables in equation (6).

2.4.1 Modification of atomic data

Model atoms are based on set of TLUSTY files (Hubeny 1988, Hubeny & Lanz 1992, Hubeny & Lanz 1995, Lanz & Hubeny 2003). The original set described in Paper I was extended to allow for consistent inclusion of X-rays (see Table 1). Our model atoms are based on the data derived from the Opacity Project (Seaton 1987, Fernley et al. 1987, Luo & Pradhan 1989, Sawey & Berrington 1992, Seaton et al. 1992, Butler et al. 1993, Nahar & Pradhan 1993) and Iron Project (Hummer et al. 1993, Bautista 1996, Nahar & Pradhan 1996, Zhang 1996, Bautista & Pradhan 1997, Zhang & Pradhan 1997, Chen & Pradhan 1999). For phosphorus we employed data described by Pauldrach et al. (2001).

2.4.2 Auger ionization

In addition to the direct ionization (of a valence electron), the Auger ionization can significantly alter the ionization state of a stellar wind in the presence of X-rays (see Cassinelli & Olson 1979, Olson & Castor 1981, MacFarlane et al. 1994, Pauldrach et al. 1994).

Table 1. Atoms and ions included in the NLTE calculations. Here ‘Level’ means either an individual level or a set of levels merged into a superlevel.

Ion	Levels	Ion	Levels	Ion	Levels	Ion	Levels
H I	9	O II	50	Al II	16	Ar III	25
H II	1	O III	29	Al III	14	Ar IV	19
He I	14	O IV	39	Al IV	14	Ar V	16
He II	14	O V	14	Al V	16	Ar VI	11
He III	1	O VI	20	Al VI	1	Ar VII	1
C II	14	O VII	1	Si II	12	Ca II	16
C III	23	Ne II	15	Si III	12	Ca III	14
C IV	25	Ne III	14	Si IV	13	Ca IV	20
C V	11	Ne IV	12	Si V	15	Ca V	22
C VI	1	Ne V	17	Si VI	1	Ca VI	1
N II	14	Ne VI	11	P III	16	Fe III	29
N III	32	Ne VII	1	P IV	17	Fe IV	32
N IV	23	Na II	13	P V	21	Fe V	30
N V	13	Na III	14	P VI	14	Fe VI	27
N VI	15	Na IV	18	P VII	1	Fe VII	1
N VII	1	Na V	16	S II	14	Ni III	36
		Na VI	1	S III	10	Ni IV	38
		Mg III	14	S IV	18	Ni V	48
		Mg IV	14	S V	14	Ni VI	1
		Mg V	13	S VI	16		
		Mg VI	1	S VII	1		

To include the Auger ionization we inserted Auger photoionization terms into statistical equilibrium equations (6),

$$\sum_{j \neq i} N_j P_{ji} - N_i \sum_{j \neq i} P_{ij} - N_i \sum_{j > i} R_{ij}^{\text{Auger}} = 0, \quad (7)$$

where R_{ij}^{Auger} is the Auger photoionization rate with j corresponding to the ground level of higher ions. Introducing the notation $\text{ion}(i)$, which means the ionization state, to which the level i belongs, the Auger photoionization rate is given as a product

$$R_{ij}^{\text{Auger}} = a_{\text{ion}(i)\text{ion}(j)} R_{\text{ion}(i)}^{\text{Auger}}, \quad (8)$$

where $a_{\text{ion}(i)\text{ion}(j)}$ is the Auger yield, i.e., the probability that $\text{ion}(j) - \text{ion}(i)$ electrons are expelled due to the Auger ionization of ionic state $\text{ion}(i)$, i.e. that ionization state $\text{ion}(j)$ is created during the process of Auger ionization, and $R_{\text{ion}(i)}^{\text{Auger}}$ is the total inner-shell photoionization rate of $\text{ion}(i)$. The total inner-shell photoionization rate is given as a sum of partial inner-shell photoionization rates from all closed inner shells. Auger rates for transitions ending in the ionization states which are not included in statistical equilibrium equations are assumed to contribute to the closest lower ionization state considered. The term corresponding to the Auger ionization is also included in the absorption coefficient in the continuum part of the radiative transfer equation.

The influence of Auger ionization on the temperature and the photon emission due to Auger ionization are neglected.

Photoionization cross sections from individual inner-shells were taken from Verner & Yakovlev (1995, see also Verner et al. 1993) and Auger yields were taken from Kaastra & Mewe (1993).

2.4.3 Accelerated lambda iterations

Iterative solution of the radiative transfer equation together with the statistical equilibrium equations may in some cases cause numerical problems with convergence (see Hubeny 2003 for a review). To avoid these problems, we included accelerated lambda iterations into our models. Their inclusion is based on the method

proposed by Rybicki & Hummer (1992). The linearization of derived equations is based on Newton-Raphson iterations. Thus, our method resembles approximate Newton-Raphson method of Hempe & Schönberg (1986). The statistical equilibrium equation (6) have for each i the form of

$$\begin{aligned} & \sum_{j<i} 4\pi N_j \int_{\nu_j}^{\infty} \frac{\alpha_{j,\nu}}{h\nu} J_\nu d\nu + \\ & + \sum_{j>i} 4\pi N_j \left(\frac{N_i}{N_j}\right)^* \int_{\nu_i}^{\infty} \frac{\alpha_{i,\nu}}{h\nu} \left[\frac{2h\nu^3}{c^2} + J_\nu\right] e^{-\frac{h\nu}{kT_e}} d\nu - \\ & - \sum_{j<i} 4\pi N_i \left(\frac{N_j}{N_i}\right)^* \int_{\nu_j}^{\infty} \frac{\alpha_{j,\nu}}{h\nu} \left[\frac{2h\nu^3}{c^2} + J_\nu\right] e^{-\frac{h\nu}{kT_e}} d\nu - \\ & - \sum_{j>i} 4\pi N_i \int_{\nu_i}^{\infty} \frac{\alpha_{i,\nu}}{h\nu} J_\nu d\nu + \sum_{j\neq i} N_j \tilde{P}_{ji} - N_i \sum_{j\neq i} \tilde{P}_{ij} = 0, \end{aligned} \quad (9)$$

where we explicitly write rates of direct radiative ionization (I.7a) and recombination (I.7b), $\alpha_{i,\nu}$ is the photoionization cross-section from level i with threshold frequency ν_i (similarly for $\alpha_{j,\nu}$), J_ν is the mean continuum intensity, T_e is the electron temperature, asterisk denotes an LTE value and \tilde{P}_{ij} are rates of all remaining transitions (collisional ionization, recombination, excitation and deexcitation (I.8) and radiative bound-bound transitions, equations (I.3), (I.5), (I.14), and the Auger ionization (8)).

Introducing the quantity U_{ji} as

$$U_{ji} = n_H z_{\text{atom}} \left(\frac{N_i}{N_j}\right)^* \alpha_{i,\nu} \frac{2h\nu^3}{c^2} e^{-\frac{h\nu}{kT_e}}, \quad (10)$$

the free-bound emissivity has the form of

$$\eta_\nu = \sum_{ij, j>i} N_j U_{ji}, \quad (11)$$

where n_H is the hydrogen number density and z_{atom} is abundance (number densities ratio) of a given atom relative to the hydrogen. During the process of the solution of the radiative transfer equation we derive the mean intensity J_ν from the emissivity (11) as follows. Using vector quantities $\mathbf{J}_\nu = (J_\nu^1, J_\nu^2, \dots, J_\nu^{NR})^T$ and $\boldsymbol{\eta}_\nu = (\eta_\nu^1, \eta_\nu^2, \dots, \eta_\nu^{NR})^T$, where NR is considered number of depth points, the radiative transfer equation for a given frequency can be expressed in a symbolic form as

$$\mathbf{J}_\nu = \Psi_\nu [\boldsymbol{\eta}_\nu], \quad (12)$$

where the matrix operator Ψ_ν represents solution of the radiative transfer equation. However, the actual process of solution is different, we do not apply the operator Ψ_ν on $\boldsymbol{\eta}_\nu$, but the mean intensity J_ν is derived as the solution of linear set of equations

$$\boldsymbol{\eta}_\nu = \Psi_\nu^{-1} [\mathbf{J}_\nu], \quad (13)$$

which is in fact the formal solution of the radiative transfer equation. Hence, during the solution of the radiative transfer equation (13) we do not know an explicit form of Ψ_ν , but we know its inversion Ψ_ν^{-1} . Since for the acceleration of convergence of statistical equilibrium equations (6) together with the continuum radiative transfer equation (13) we need to know derivatives $\partial J_\nu / \partial N_j$, we consequently need to know the explicit form of Ψ_ν . However, because for the solution of equations of statistical equilibrium we use only derivatives of mean intensity with respect of N_j at a given depth point, we need to know only the diagonal part of the operator Ψ_ν (see equation (11)). This significantly reduces the necessary computer power. Note that because we use LAPACK package (<http://www.cs.colorado.edu/~lapack>, Anderson

et al. 1999) for the solution of radiative transfer equation (13), which is based on LU decomposition, we can easily calculate diagonal elements of Ψ_ν (see Appendix A). Finally, derivatives of mean intensities inserted into the statistical equilibrium equations have at the depth point IR the approximate form of

$$\left. \frac{\partial J_\nu}{\partial N_i} \right|_{IR} \approx \Psi_{\nu, IR, IR} U_{ij}, \quad (14)$$

where $\Psi_{\nu, IR, IR}$ is the corresponding diagonal element of Ψ_ν at a depth point IR and U_{ij} was defined in equation (10).

During the iterative solution of statistical equilibrium equations we solve for the corrections δN_i to the actual relative occupation numbers N_i . These corrections are calculated using equation (I.22). Here we also add corrections due to the dependence of the mean intensity on N_i (equation 14). Hence, instead of equations (I.22) we solve (compare with equation 9)

$$\begin{aligned} & \sum_{j<i} 4\pi N_j \int_{\nu_j}^{\infty} \frac{\alpha_{j,\nu}}{h\nu} \Psi_{\nu, IR, IR}^* U_{ij} \delta N_i d\nu + \\ & + \sum_{j>i} 4\pi N_j \left(\frac{N_i}{N_j}\right)^* \int_{\nu_i}^{\infty} \frac{\alpha_{i,\nu}}{h\nu} \Psi_{\nu, IR, IR}^* U_{ji} \delta N_j e^{-\frac{h\nu}{kT_e}} d\nu - \\ & - \sum_{j<i} 4\pi N_i \left(\frac{N_j}{N_i}\right)^* \int_{\nu_j}^{\infty} \frac{\alpha_{j,\nu}}{h\nu} \Psi_{\nu, IR, IR}^* U_{ij} \delta N_i e^{-\frac{h\nu}{kT_e}} d\nu - \\ & - \sum_{j>i} 4\pi N_i \int_{\nu_i}^{\infty} \frac{\alpha_{i,\nu}}{h\nu} \Psi_{\nu, IR, IR}^* U_{ji} \delta N_j d\nu + \\ & + \sum_{j\neq i} \left[N_j \frac{\partial P_{ji}}{\partial N_i} \delta N_i + \left(P_{ji} + N_j \frac{\partial P_{ji}}{\partial N_j} \right) \delta N_j \right] - \\ & - \sum_{j\neq i} \left[\left(P_{ij} + N_i \frac{\partial P_{ij}}{\partial N_i} \right) \delta N_i + N_i \frac{\partial P_{ij}}{\partial N_j} \delta N_j \right] = 0, \end{aligned} \quad (15)$$

where first four sums represent the term of accelerated lambda iterations and the meaning of other terms is the same as in Paper I.

Finally, for the calculation of continuum mean intensities J_ν (see equation 13) we use the formal solution (i.e. for given opacity and emissivity) of the momentum form of the radiative transfer equation with inclusion of sphericity factors (Auer 1971).

To accelerate the convergence even more, we have also included the Ng acceleration (Ng 1974, see also Auer 1987 or Hubeny 2003).

3 STUDIED STARS

This paper studies the influence of X-rays on the basic parameters of radiatively driven stellar winds. However, to avoid using of ad hoc stellar parameters, we rather decided to choose a set of parameters corresponding to real stars with basic parameters already known to some degree of accuracy.

3.1 Stellar parameters

Our study is based on O stars with effective temperatures $T_{\text{eff}} \lesssim 40\,000$ K, which were detected by *ROSAT* satellite as X-ray sources (Berghöfer et al. 1996, hereafter BSC). They were selected out of stars studied by Repolust et al. (2004, hereafter R04), Markova et al. (2004, hereafter M04), and in the Paper I. To enlarge our dataset we also included such stars from Martins et al. (2005, hereafter M05) sample, for which measured X-ray fluxes are available in the literature. All but one of these stars exhibit the so-called "weak

Table 2. Stellar parameters of selected O stars. Stars exhibiting the "weak wind problem" appear in the bottom part below the horizontal line. Spectral types are taken from the Simbad database.

Star	HD number	Sp. type	R_* [R_\odot]	M [M_\odot]	T_{eff} [K]	Source
ξ Per	24912	O7.5IIIe	14.0	36	35 000	R04
α Cam	30614	O9.5Iae	27.6	43	30 900	LSL
λ Ori A	36861	O8 III	12.3	30	36 000	LSL
	54662	O7III	11.9	38	38 600	M04
	93204	O5V	11.9	41	40 000	M05
ζ Oph	149757	O9V	8.9	21	32 000	R04
63 Oph	162978	O8III	16.0	40	37 100	LSL
68 Cyg	203064	O8e	15.7	38	34 500	R04
19 Cep	209975	O9Ib	22.9	47	32 000	R04
λ Cep	210839	O6Iab	19.6	51	38 200	LSL
<hr/>						
AE Aur	34078	O9.5Ve	7.5	20	33 000	M05
μ Col	38666	O9.5V	6.6	19	33 000	M05
	42088	O6.5V	9.6	31	38 000	M05
	46202	O9V	8.4	21	33 000	M05

wind problem", i.e., their theoretically predicted mass-loss rates are significantly higher than those derived from observations.

Adopted parameters of studied O stars are given in Table 2. Effective temperatures and radii are taken from R04, M04, M05, and Lamers et al. (1995, hereafter LSL). Parameters derived by R04, M04, and M05 were obtained using blanketed model atmospheres, i.e., they are more reliable than the older ones. Stellar masses were obtained using evolutionary tracks either by us (using tracks calculated by Schaller et al. 1992) or by LSL or M05. The use of the evolutionary masses instead of the spectroscopic ones may cause a systematic shift due to the well-known discrepancy between these masses (e.g. Herrero et al. 1992). However, for many stars from our sample these masses are nearly the same.

3.2 Wind parameters derived from observations

Wind parameters of studied stars (both derived from observations and predicted ones) are given in Table 3.

X-ray luminosities, which are assumed to originate in the wind, were taken from BSC with an exception of stars HD 42088, HD 46202, and HD 93204, for which the X-ray luminosities were taken from Chlebowski & Garmany (1991) and Evans et al. (2003).

Because there is still no broad consensus about the influence of clumping on mass-loss rates derived from observations, we used mass-loss estimations from Puls et al. (2006b, hereafter P06), which were regarded as upper limits with respect to clumping, supplemented by results of M05. Although M05 derived mass-loss rates of some stars with inclusion of clumping, for most stars selected by us from this sample the clumping factor was set by them to one, because these stars exhibit the "weak wind problem". The only exception is the star HD 93204, for which M05 provide mass-loss rate with clumping taken into the account. However, to keep our sample more compact, we used mass-loss rate uncorrected for clumping (calculated as $\dot{M}/\sqrt{f_\infty}$, where f_∞ is the clumping factor in the outer wind derived by M05). Because P06 concluded that mass-loss rates derived from radio data are less influenced by clumping, for the star HD 149757 we adopted such rates derived by Lamers & Leitherer (1993).

Terminal wind velocities were taken from LSL, Puls et al. (1996), and M04 (the uncertainties were either taken from LSL or

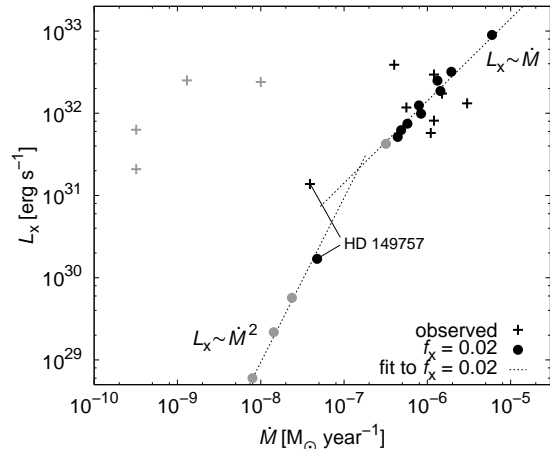


Figure 1. The relation between L_X and \dot{M} plotted using wind parameters derived from observations and from theoretical models ($f_X = 0.02$). The relations $L_X \sim \dot{M}$ for stars with optically thick winds in the outer regions (stars with large mass-loss rates) and $L_X \sim \dot{M}^2$, valid for stars with optically thin winds (OC) are also plotted in the graph (dotted lines). Gray symbols denote values for stars exhibiting "weak wind problem".

calculated assuming 10% errors as suggested by Puls et al. 1996). For stars that exhibit the "weak wind problem" the terminal velocities derived from observations may be just lower limits, similarly as in Martins et al. (2004). Consequently, we did not consider the terminal velocities of these stars in the following analysis.

4 THE EMERGENT X-RAYS

4.1 The L_X/L relation

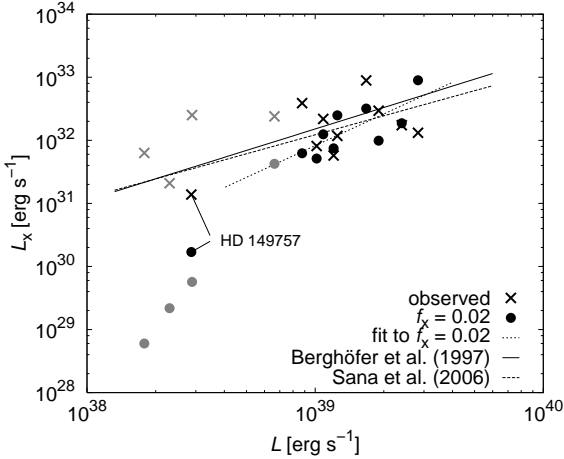
From the analytic considerations Owocki & Cohen (1999, hereafter OC) showed that the optically thin X-ray luminosity depends on the square of the mass-loss rate $L_X \sim (\dot{M}/v_\infty)^2$, whereas the X-ray luminosity of the optically thick wind scales linearly with the mass-loss rate $L_X \sim \dot{M}/v_\infty$. A slightly different form of these relations can be expected due to the assumed dependence of the shock temperature T_X on the wind terminal velocity. Consequently, in the following we use simpler relations $L_X \sim \dot{M}^2$ for the optically thin wind in the X-ray region and $L_X \sim \dot{M}$ for the optically thick wind. From the relation $\dot{M} \sim L^{1/\alpha'}$ (Kudritzki & Puls 2000), where $\alpha' = \alpha - \delta$ and α and δ are usual CAK force multipliers, the X-ray luminosity of optically thick wind is predicted to be proportional to $L_X \sim L^{1/\alpha'}$ ($\alpha' \approx 0.5$).

However, from the observations a slightly different trend emerges, because the observed X-ray luminosity L_X is roughly linearly proportional to the total luminosity L (e.g. Chlebowski et al. 1989; Berghöfer et al. 1996; Sana et al. 2006). The origin of the difference is not clear. OC suggested that the observed relation can be reproduced assuming that f_X decreases with radius.

To understand the origin of L_X/L relation we calculated wind models with a fixed filling factor. To be specific, we chose $f_X = 0.02$. In agreement with the calculations of OC, the X-ray luminosity of individual stars depends mostly on the wind mass-loss rate (see Fig. 1). Stars with large mass-loss rates $\dot{M} \gtrsim 10^{-7} M_\odot \text{ yr}^{-1}$ have an optically thick wind in the X-ray domain (between the outermost model point and the region where most of the X-rays are generated) and the X-ray luminosity of theoretical models calcu-

Table 3. Wind and X-ray parameters of studied O stars. Wind parameters derived from observation are described in Sect. 3.2. Predicted wind parameters were derived using our NLTE models with different properties of X-ray sources (models with $f_X = 0$, $f_X = 0.02$ and $u_{\text{rel}} = 0.3$).

HD number	log L_X [CGS]	Observed		Predicted no X-rays		Predicted – $f_X = 0.02$		
		\dot{M} [$M_\odot \text{ yr}^{-1}$]	v_∞ [km s^{-1}]	\dot{M} [$M_\odot \text{ yr}^{-1}$]	v_∞ [km s^{-1}]	log L_X [CGS]	\dot{M} [$M_\odot \text{ yr}^{-1}$]	v_∞ [km s^{-1}]
24912	31.91	1.2×10^{-6}	2450	4.4×10^{-7}	2270	31.71	4.4×10^{-7}	2750
30614	32.24	1.5×10^{-6}	1500	1.5×10^{-6}	1950	32.27	1.4×10^{-6}	2290
36861	32.59	4×10^{-7}	2200	4.8×10^{-7}	2150	31.80	4.8×10^{-7}	2500
54662	32.34		2450	7.9×10^{-7}	2190	32.10	7.9×10^{-7}	2480
93204	32.07	5.6×10^{-7}	2900	1.3×10^{-6}	2290	32.40	1.3×10^{-6}	2400
149757	31.14	3.9×10^{-8}	1550	4.7×10^{-8}	2040	30.23	4.7×10^{-8}	2280
162978	32.95		2200	2.0×10^{-6}	2040	32.50	1.9×10^{-6}	2190
203064	31.76	1.1×10^{-6}	2550	5.7×10^{-7}	2080	31.87	5.8×10^{-7}	2590
209975	32.47	1.2×10^{-6}	2050	8.4×10^{-7}	2430	31.99	8.4×10^{-7}	2900
210839	32.12	3.0×10^{-6}	2200	6.1×10^{-6}	1990	32.95	6.0×10^{-6}	1910
34078	31.32	3.2×10^{-10}	800	1.4×10^{-8}	2950	29.34	1.4×10^{-8}	3490
38666	31.80	3.2×10^{-10}	1200	7.9×10^{-9}	4380	28.78	8.0×10^{-9}	4480
42088	32.38	1×10^{-8}	1900	3.1×10^{-7}	2180	31.63	3.2×10^{-7}	2680
46202	32.40	1.3×10^{-9}	1200	2.3×10^{-8}	1900	29.76	2.4×10^{-8}	2890

**Figure 2.** The relation between the X-ray luminosity L_X and the total luminosity L for studied stars calculated assuming $f_X = 0.02$. Overplotted are the average observed relations derived by Berghöfer et al. (1997), Sana et al. (2006), observed values for studied stars, and the linear fit to the theoretical expectations (only for stars with thick winds). Gray symbols denote values for stars exhibiting “weak wind problem”.

lated with a fixed f_X depends on \dot{M} linearly. On the other hand, stars with low mass-loss rates $\dot{M} \lesssim 10^{-7} M_\odot \text{ yr}^{-1}$ have optically thin wind and their theoretical X-ray luminosity depends on \dot{M}^2 .

The $L_X - \dot{M}$ relation plotted using wind parameters derived from observations (Fig. 1) is different. The correlation between the observed mass-loss rate and X-ray luminosity is less apparent. Moreover, the observed X-ray luminosities for stars with low mass-loss rates $\dot{M} \lesssim 10^{-7} M_\odot \text{ yr}^{-1}$ lie considerably above the theoretical expectations. These stars have nearly the same L_X as stars with high mass-loss rates.

The predicted dependence of L_X on L displayed in Fig. 2 reflects the dependence of L_X on \dot{M} . For stars with dense winds, i.e., for stars with large luminosities ($L \gtrsim 5 \cdot 10^{38} \text{ erg s}^{-1}$) the X-ray luminosity scales as \dot{M} , and due to the dependence of \dot{M} on L , L_X depends mostly on the stellar luminosity as $L_X \sim L^{1.7}$. This

is in agreement with scaling $L_X \sim L^{1/\alpha'}$ where $\alpha' \approx 0.6$. For stars with thick winds these models roughly recover the observed L_X/L relation. Remaining difference between predicted slope of L_X/L relation and the observed one may be either due the radial dependence of the filling factor (as proposed by OC), or due to the dependence of the filling factor on wind density (Sect. 8.1). Higher scatter of the observed X-ray luminosities may be partly caused by poorly known distances (cf. with the results of Sana et al. 2006).

For stars with lower luminosities, $L \lesssim 5 \cdot 10^{38} \text{ erg s}^{-1}$, there is an abrupt change in L_X/L relation derived from our models with fixed f_X . These stars have optically thin wind, and their X-ray luminosities scale as $L_X \sim \dot{M}^2$. Because the mass-loss rate depends mainly on the stellar luminosity, the L_X/L relationship derived from theoretical models consequently steepens. However, the observed X-ray luminosities are much higher than the predicted ones. The observational L_X/L relation is almost the same for both groups of stars with optically thick and thin winds. Because in the case of optically thin winds we observe basically all X-rays emitted, our description of shock properties of these stars is likely oversimplified. Other possibilities, like different heating mechanism (e.g., wind frictional heating, Kubát et al. 2004) are also not ruled out.

The enhanced X-ray activity may not be limited only to the stars exhibiting the “weak wind problem”. From observations of Berghöfer et al. (1997) follows that also many other late O main sequence stars show X-ray luminosity corresponding to the stars with thick winds.

4.2 The radial distribution of X-ray emissivity

Most of X-rays in our models are generated close to the star, as shown in the plot of radial variations of X-ray emissivity Fig. 3. Due to assumed dependence of the shock temperature on wind velocity (via equations (1), (3)), the X-ray emissivity is increasing function of radius close to the star. On the other hand, we assume that the X-ray emissivity depends on the square of the wind density (see equation (4)), consequently the emissivity decreases in the outer regions.

For stars with optically thick wind only a very small part of generated X-rays finally escapes the wind and may reach a distant observer, as can be seen from the difference between the radii at

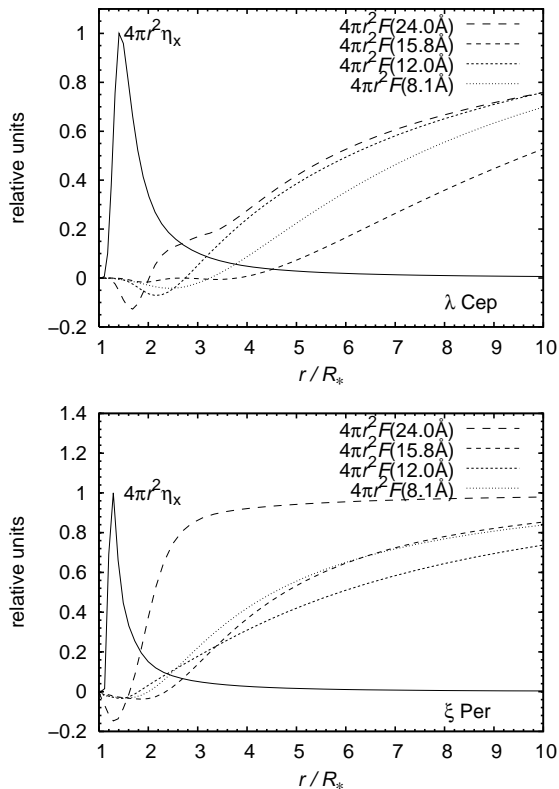


Figure 3. The radial dependence of the total shock emissivity (integrated over frequencies and plotted as $4\pi r^2 \eta_X$) and the monochromatic luminosity $4\pi r^2 F(\lambda)$ for $f_X = 0.02$ for stars λ Cep and ξ Per. The quantities are plotted relatively to their maximum values. Note that the integrated emissivity has maximum below the radius at which the X-ray luminosities reach the observed value. This indicates that most of X-rays emitted in the wind do not escape.

which $4\pi r^2 \eta_X$ has maximum and at which the monochromatic luminosities approach the terminal value in Fig. 3. Due to the continuum X-ray absorption also the X-ray luminosity of optically thick wind depends less steeply on the wind mass-loss rate than the X-ray luminosity of optically thin wind (see Fig. 1 and OC). The X-ray flux is not always monotonically increasing, and in some regions it is even negative due to the transfer of part of emitted X-rays towards the stellar surface.

In the outer regions the monochromatic luminosities $4\pi r^2 F(\lambda)$ in Fig. 3 rise and reach the value measured by a distant observer as the wind becomes optically thin. Waldron & Cassinelli (2007) showed that there is a correlation between the radius R_{fir} of the formation of forbidden intercombination resonance (*fir*) lines of He-like ions derived from observations, and the radius at which the continuum optical depth at associated wavelength is unity. Note, however, that the formation radius of the observed X-rays depends not only on opacity (optical depth), as Waldron & Cassinelli (2007) stressed, but naturally also on emissivity. Consequently, we argue that the relationship found by Waldron & Cassinelli (2007) is more precisely manifested as a correlation between R_{fir} and the radius $R_{1/2}$ at which the monochromatic luminosity at the associated wavelength is equal to half of its terminal value (Fig. 4).

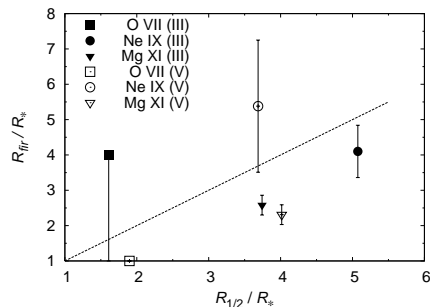


Figure 4. The relation between the radius R_{fir} of the formation of *fir* lines of He-like ions derived from observations by Waldron & Cassinelli (2007) and the radius $R_{1/2}$ at which the monochromatic luminosity is equal to half of its terminal value (for $f_X = 0.02$). The radii derived for individual lines for giants (III) and main-sequence stars (V) are plotted using different symbols. Dashed line denotes one to one relation.

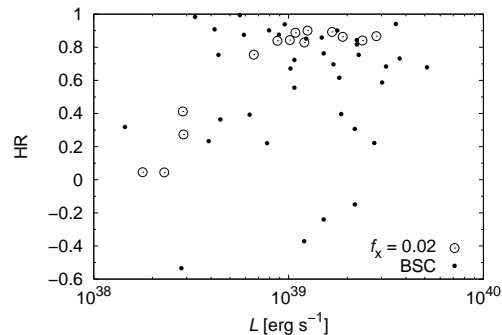


Figure 5. The comparison between observed (derived by BSC for O stars) and model hardness ratio defined by equation (16).

4.3 The hardness ratio

To test whether the derived spectral energy distribution of X-rays is at least roughly correct, we compare the predicted and observed hardness ratio, introduced by BSC as

$$\text{HR} = (\text{H} - \text{S})/(\text{H} + \text{S}), \quad (16)$$

where H and S are the integrated fluxes in the hard (0.5 – 2.0 keV) and soft (0.1 – 0.4 keV) energy bands, respectively (see Fig. 5). The model hardness ratio is nearly constant for stars with large luminosities. It decreases for stars with lower luminosities, because the stellar wind of these stars is less opaque and regions close to the star (where X-rays with lower energies are generated) become visible. The observed values for many stars are, however, lower than the predicted ones and display larger scatter. In the frame of our model this means that the observations cannot be explained just by a single value of u_{rel} .

5 INFLUENCE OF X-RAYS ON THE IONIZATION STATE

Although not directly observable, ionization structure of the wind gives us a useful direct insight to the effect of different radiation processes in the stellar atmosphere and wind. In our models the X-rays affect wind ionization structure via direct and Auger ionization (MacFarlane et al. 1994, Pauldrach et al. 1994).

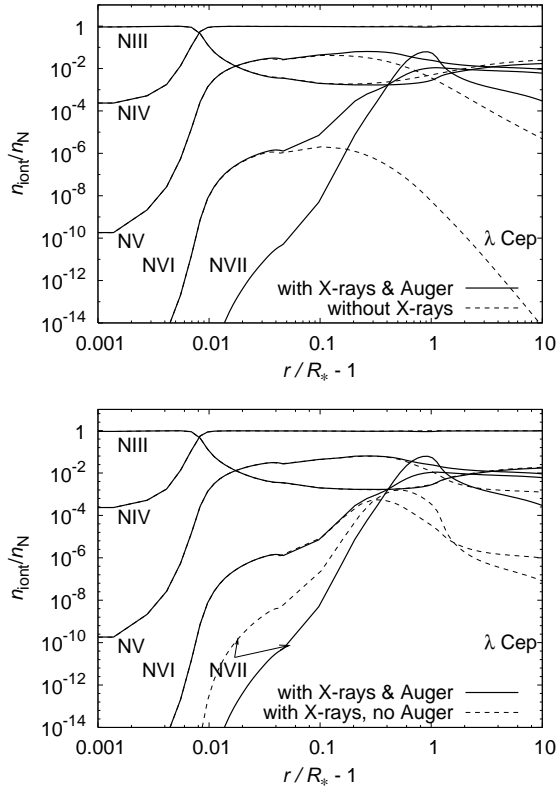


Figure 6. Radial variation of nitrogen ionization fractions in the wind model of λ Cep for $f_X = 0.0028$ that fits the observed L_X . *Top panel:* Comparison of models calculated with additional X-ray sources (solid lines) and without these sources (dashed lines). *Bottom panel:* Comparison of models with additional X-ray sources calculated with inclusion of Auger processes (solid lines) and neglecting the Auger processes (dashed lines). For better readability, the ionization fraction of N II is not plotted.

5.1 Radial variations of the ionization fractions

As an example we discuss the variations of nitrogen ionization in the case of the star λ Cep (HD 210839). To understand the influence of individual ionization mechanisms on the wind ionization structure we also calculated models without additional X-ray sources and models which take these sources into account, but which neglect Auger processes (see Figs. 6 for the plot of the variations of nitrogen ionization fractions with the radius).

The ionization fractions of most abundant ions (N III, N IV) close to the stellar surface are not significantly influenced by the additional sources of X-rays. This region is optically thick for the X-ray radiation and only a very tiny amount of X-rays emitted in the highly supersonic wind parts may penetrate close to the stellar surface and modify the ionization fractions of minor higher ions there (in our case N VI and N VII). With increasing radius (for $r/R_* - 1 \gtrsim 0.1$) the wind becomes more ionised due to lower wind density, and X-rays start to play a more important role in the ionization balance. As a result of our assumptions, the Auger ionization significantly influences the ionization balance only in the outer wind regions. This is caused by the fact that more energetic X-rays emitted in the wind with sufficiently high velocity are necessary for the Auger ionization than for direct ionization.

The ionization fraction of N V is increased due to direct ionization from N IV and is influenced also by ionization to and recombination from N VI. The ionization fraction of N VI is increased by

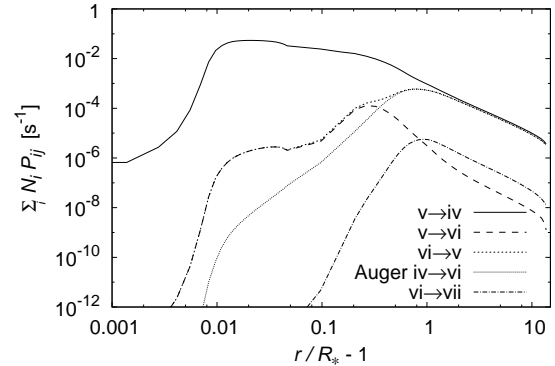


Figure 7. The radial dependence of selected sums of radiative ionization/recombination rates $\sum_i N_i P_{ij}$ in the model of λ Cep ($f_X = 0.0028$). Rates are summed over all transitions between corresponding ions. Close to the star, the ionization fraction of N V is given by the radiative ionization balance with N IV. In the outer regions also the recombination from N VI influences the fraction of N V. Consequently, N V partly occurs due a two-step process (Auger ionization of N IV followed by the radiative recombination).

both Auger and direct ionization. N VII is generated due to the direct ionization of N VI (see Fig. 7).

The result that for $r/R_* - 1 \lesssim 0.5$ the ionization fraction of N VII is higher in the case of neglected Auger processes than in the model with these processes may seem paradoxical, but it has a simple explanation. In the case of neglected Auger processes the stellar wind is less opaque in the X-ray region and, consequently, the intensity of X-ray radiation is higher. Because N VII is created via direct ionization of N VI, the ionization fraction of N VII is higher.

5.2 Variations with the effective temperature

To compare the ionization equilibrium for different stars, we plot the ionization fractions of selected ions for the points where the wind velocity is equal to $v_r = 0.5v_\infty$ (Fig. 8). The model predictions are compared with the ionization fractions derived from observations by Howarth & Prinja (1989), Lamers et al. (1999) for Galactic stars, and Massa et al. (2003) for stars from the Large Magellanic Cloud. Stars from the Clouds have generally lower metallicity than the Galactic ones (e.g. Martins et al. 2004). However, because the dependence of ionization fractions on metallicity is not strong, we use also these fractions for our comparison.

The ionization fractions are influenced not only by the stellar effective temperature and by local wind parameters, but also by the amount of additional ionizing X-rays. Consequently, the variations plotted in Fig. 8 are far from being monotonic. In agreement with MacFarlane et al. (1994), the ionization fractions of the dominant ions are usually not influenced by X-ray emission. X-rays above all modify the ionization fractions of minor higher ionization states of a particular atom both due to the direct and Auger ionization. There is a satisfactory agreement between our results and models of MacFarlane et al. (1994). Note the influence of X-rays on the ionization balance already very deep in the wind as both observational and theoretical results show relatively large amount of O VI close to the stellar surface for $v_r = 0.05 v_\infty$ (Fig. 9). However, X-rays do not alter the ionization state of the dominant and of the lower neighbouring ions there (cf., Fig. 6).

The influence of X-rays on the ionization structure is stronger

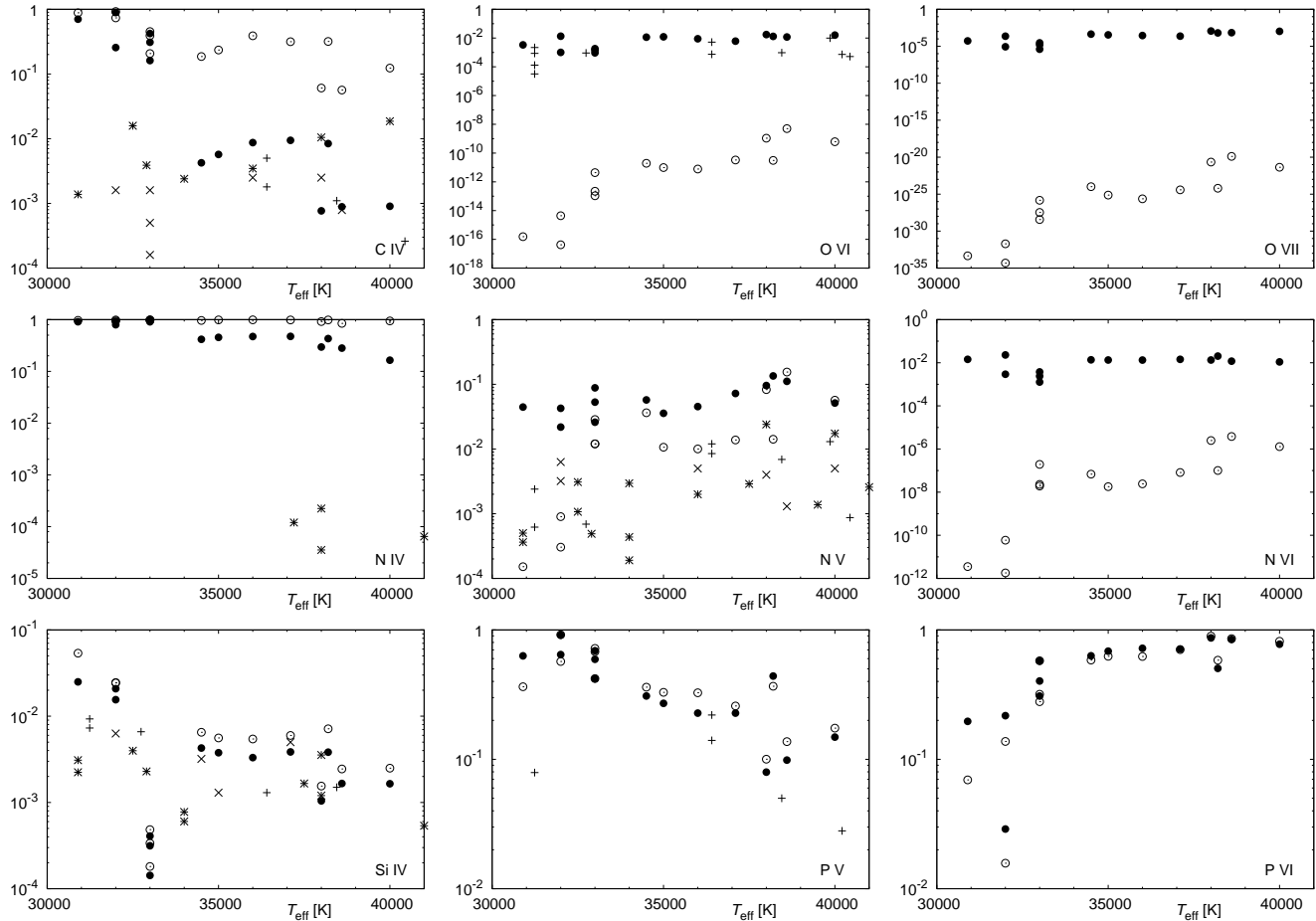


Figure 8. Ionization fractions as a function of the effective temperature for individual stars from our sample at the point where the radial velocity $v_r = 0.5v_\infty$. Open circles \odot denote values taken from models without X-ray radiation, filled circles \bullet from models with $f_X = 0.02$. The ionization fraction derived from observations were adopted from Massa et al. (2003, for LMC stars, plus signs +), Howarth & Prinja (1989, only for stars from our sample, crosses \times), and Lamers et al. (1999, asterisks *).

for stars with less dense winds and for stars with weaker flux of the ionizing radiation, i.e. for cooler stars.

The presence of N V lines in the wind spectra is a frequently used argument for the existence of an additional source of ionization. However, as we can see from the comparison of the ionization structure derived from observations and from our models for $v = 0.05v_\infty$, and $v = 0.5v_\infty$ (Figs. 9, 8), the ionization fraction of N V there can be explained just by the detailed NLTE models without a contribution of X-ray radiation. This was shown already by Pauldrach (1987). Only the presence of N V in a significant amount at higher wind speeds (see Fig. 10 and also Fig. 6) is caused by the existence of a strong X-ray source.

5.3 Phosphorus

The failure of present NLTE wind models to reproduce the ionization fractions of P V derived from observations is one of the main arguments for lower values of wind mass-loss rates. There is large discrepancy between P V ionization fraction derived by us and those derived from observations by Fullerton et al. (2006), who concluded that either on average the ionization fraction of P V is lower than 0.1 or there is a significant disagreement between mass-loss rates derived from P V and H α lines. Some part of this discrep-

ancy may come from the neglected influence of inhomogeneities on the wind ionization fractions or radiative transfer (Puls et al. 2006a; Krtićka et al. 2007; Oskinova et al. 2007). Anyway, it is worthwhile to understand whether some part of this discrepancy is not caused by the fact that P V is a fragile ion, which is not a dominant one for any effective temperature, and to test the influence of X-rays on P V ionization fraction.

Our calculations show that P V is a dominant ion in the inner part of the wind only for stars with $T_{\text{eff}} \lesssim 34\,000$ K (in accordance with theoretical results discussed by Fullerton et al. 2006, see right lower panels of Fig. 8 for the predicted ionization fraction of P V and P IV). For hotter stars also P VI becomes an important ionization stage. However, the presence of shock X-ray radiation does not significantly modify the ionization fraction of P V. Consequently, even for hotter stars for which P V is not a dominant ion there is a significant discrepancy between theoretical and observational results, as can be seen from Fig. 11. Here we plot the values, which can be in fact derived from observations, i.e. the product of the ionization fraction and the mass-loss rate $q_{\text{P V}} \dot{M}$, and compare it with the predicted ones. For hotter stars ($T_{\text{eff}} \gtrsim 35\,000$ K), the predicted values are on average by a factor of 7 higher than those derived from observations (with an exception of the star HD 42088, which displays the “weak wind problem”). On the other hand, for cooler

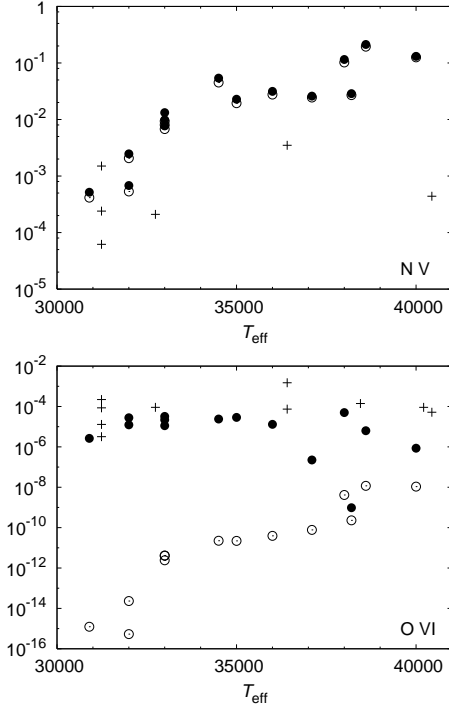


Figure 9. The same as Fig. 8, however for $v_r = 0.05v_\infty$.

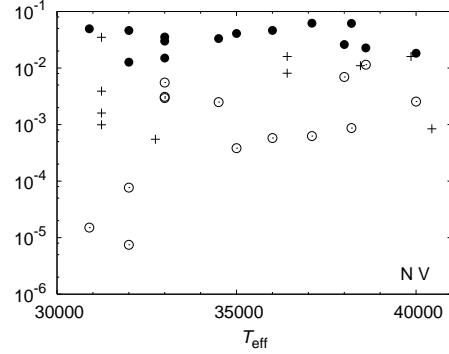


Figure 10. The same as Fig. 8, however for $v_r = 0.8v_\infty$.

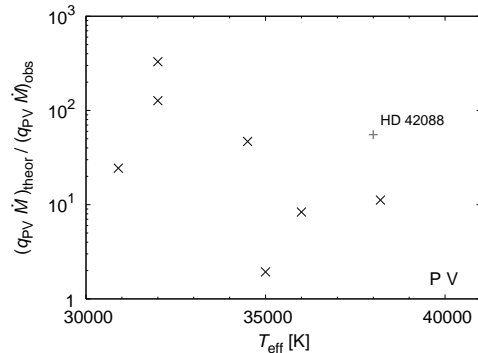


Figure 11. Comparison of the product of the P V ionization fraction and the wind mass-loss rate derived from observations (Fullerton et al. 2006) and predicted ones (for $v_r = 0.5v_\infty$ and $f_X = 0.02$). The predicted quantities are much higher than the observed ones. Gray plus symbol corresponds to the star HD 42088, that exhibits the “weak wind problem”.

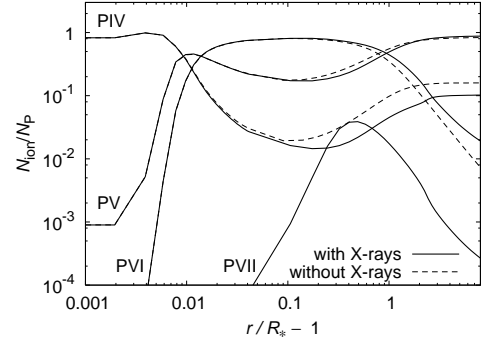


Figure 12. The influence of X-rays on the radial variations of phosphorus ionization fractions in the wind model of the star HD 203064. Note that X-rays do not significantly change P V ionization fraction and that P V dominates for $r \gtrsim 2R_*$.

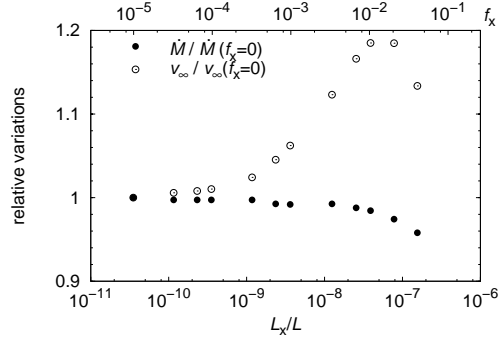


Figure 13. Variations of the mass-loss rate \dot{M} and the terminal velocity v_∞ of α Cam with f_X and L_X (L_X depends linearly on f_X) relative to their values derived using the models with no shock X-ray sources.

stars ($T_{\text{eff}} \lesssim 35000$ K) the predicted values are on average even about 100 times higher than those derived from observations.

The maximum frequency considered in our models (corresponding to 1.7 keV) is lower than P V inner-shell ionization energy threshold 2.2 keV. To test our results, we calculated also models with higher maximum frequency considered, i.e., corresponding to 3.7 keV (see Fig. 12). However, even in these models the Auger ionization of P V due to low flux of high energy X-rays does not significantly modify the ionization fraction of P V.

6 INFLUENCE OF X-RAYS ON HYDRODYNAMIC STRUCTURE

To understand the influence of X-rays on wind parameters, we calculated several wind models corresponding to α Cam stellar parameters, however with a different value of f_X , i.e. with a different value of X-ray luminosity. The variations of wind parameters with X-ray luminosity are shown in Fig. 13. As a consequence of assumed dependence of X-ray emissivity on f_X via equation (4), the emergent X-ray luminosity depends linearly on f_X . For lower X-ray luminosities ($L_X/L \lesssim 10^{-8}$) both mass-loss rate and terminal velocity are not significantly affected by the X-ray radiation, since the latter influences only the ionization state of minor ions (typically VI–VII). This picture changes for higher X-ray luminosities ($L_X/L \gtrsim 10^{-8}$). The mass-loss rate slightly decreases with increasing X-ray luminosity, whereas the terminal velocity slightly

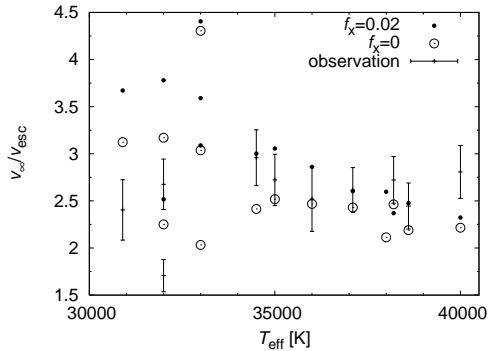


Figure 14. Comparison of the ratio v_∞/v_{esc} calculated with a theoretical value of v_∞ for $f_X = 0.02$, for neglected X-ray emission ($f_X = 0$), and the ratio v_∞/v_{esc} with v_∞ from observations (observed values for stars exhibiting weak-wind problem are excluded from this plot).

increases. Changes of wind parameters are caused by modification of ionization equilibrium due to X-rays. The X-ray radiation shifts the ionization balance to higher excited states of all elements. Because the number density of minor ionization state Fe IV, which is important for the radiative acceleration close to the star, is lowered, the radiative acceleration decreases. Consequently, the wind mass-loss rate slightly decreases in the case of α Cam.

Generally, the changes of the wind mass-loss rate due to X-rays are relatively small. The mass-loss rates for the same star calculated with f_X from 0 to 0.04 differ by no more than about 5%. This is connected with the fact that in our models the wind mass-loss rate is determined in the region close to the stellar surface below the critical point. Because this wind region is opaque to X-rays, the X-rays do not influence the ionization states significantly contributing to the radiative force there and the mass-loss rates remain basically unaltered.

The change in ionization due to the presence of X-rays does not decrease the line-force due to the lighter elements. The important lines stay optically thick and higher excited elements capable to contribute to the radiative force emerge (e.g., N V, O V, O VI). Thus, the situation in the outer wind, where the contribution of iron lines is smaller and the influence of X-rays is higher, is different. The increase of the radiative force (supported in some cases by the decrease of \dot{M}) causes the increase of the wind terminal velocity.

For stars with stronger ionizing flux in the far UV region the influence of X-rays on the wind structure is not so significant. More X-rays are necessary to modify the ionization fractions of wind driving ions. Consequently, the increase of the wind terminal velocity is larger for cooler stars ($T_{\text{eff}} \lesssim 35\,000$ K, see Fig. 14) or for stars with more tenuous winds.

The energy of artificially included X-rays also transforms to the thermal energy due to the X-ray absorption. Consequently, wind temperature may be by few thousands Kelvin higher due to X-rays. However, this effect does not significantly influence the radiative force.

7 CONSEQUENCES FOR THE X-RAY LINE TRANSFER

Using modern X-ray spectrographs it became possible to resolve the X-ray line profiles of hot stars. The study of *fir* lines of He-like ions enabled to derive radii at which the X-ray emission is generated (e.g., Kahn et al. 2001; Miller et al. 2002; Raassen et al. 2005; Leutenegger et al. 2006). It is also possible to predict the

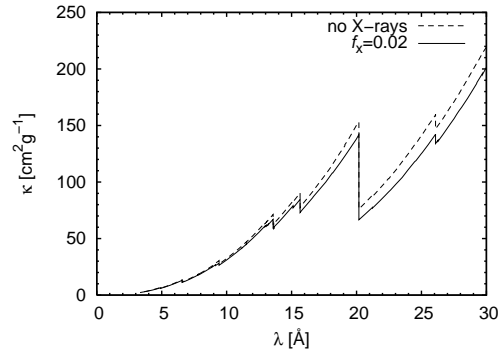


Figure 15. X-ray continuum opacity calculated with and without shock X-ray emission for ξ Per. Here we give the opacity per unit of mass averaged for the radii $1.5 R_\odot < r < 5 R_\odot$. The inclusion of X-rays leads to a slight decrease of the opacity in the X-ray region.

shapes of these X-ray lines (e.g., Owocki & Cohen 2001). Most of the predictions assume that the X-ray lines originate in the hot optically thin environment surrounded by cool wind, which is optically thick in continuum. These theoretical calculations based on currently available theoretical mass-loss rates predict asymmetric X-ray line profiles due to the wind continuum absorption. However, the observed X-ray line profiles are in most cases symmetric (e.g., Miller et al. 2002; Leutenegger et al. 2007). This either indicates that the theoretical wind mass-loss rates are overestimated or this leads to the discussion on the influence of wind inhomogeneities on the X-ray line transfer (Feldmeier et al. 2003; Owocki et al. 2004; Oskinova et al. 2006a; Owocki & Cohen 2006). Here we study the influence of modified ionization equilibrium due to hot shock emission on the line transfer in the X-ray region.

7.1 Influence of shock emission on the X-ray opacity

The theoretical prediction of the asymmetric shape of the X-ray line profiles is sensitive to the value of the opacity in the X-ray region. Krtićka & Kubát (2007) concluded that a more realistic (lower) value of adopted metallicity leads to lower continuum opacity in the X-ray region, and consequently to a better agreement between theoretical and observed X-ray line profiles. Here we test whether the ionization shift due to the presence of X-rays may affect the X-ray continuum opacity.

Our calculated opacities are in a good agreement with those presented by Oskinova et al. (2006a). Inclusion of shock X-ray emission leads to a slight decrease (on average by 8%) of the calculated opacity per unit of mass due to the ionization shift of ions He II, C V, N IV, O IV etc., as shown in Fig. 15. This could slightly improve the agreement between predicted and observed X-ray line shapes, but the decrease is too small to explain the main part of the discrepancy.

7.2 Influence of the resonance-line scattering in the cool wind on the line transfer in the X-ray region

Ignace & Gayley (2002) proposed that X-ray emitting regions may be optically thick in lines. This effect can lead to more symmetric X-ray line profiles, which better correspond to the observed ones (see also Leutenegger et al. 2007). However, the ambient cool wind is usually assumed to absorb the X-ray radiation only in continuum

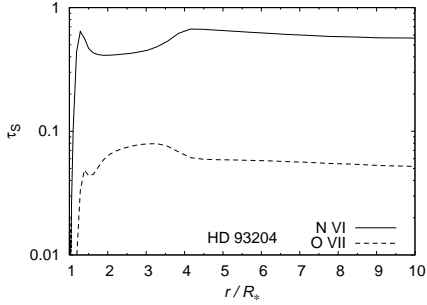


Figure 16. The Sobolev optical depth (17) due to the resonance line scattering due to $1s^2\ ^1S - 1s2p\ ^1P$ lines of helium-like ions N VI ($\lambda = 28.787\ \text{\AA}$) and O VII ($\lambda = 21.602\ \text{\AA}$) in the cool wind of HD 93204. The model was calculated for $f_X = 0.0094$ that fits the observed X-ray luminosity.

and the line absorption within the cool wind is being neglected. Here we test whether this assumption is adequate.

He-like ions N VI and O VII, whose lines are observed in the X-ray spectra of hot stars, are present in a nonnegligible amount also in a cool ambient wind (see Fig. 8). This is caused by the direct and Auger ionization of corresponding less ionised ions. The influence of the resonance-line scattering in the *cool* ambient wind on the profiles of X-ray lines emitted in shocks can be estimated from the optical depth of these lines in the cool wind. Neglecting the occupation number of upper level $n_i/g_i \gg n_j/g_j$, the Sobolev optical depth in a given line is within the radial streaming approximation roughly given by (e.g., Castor 1974)

$$\tau_S = \frac{\pi e^2}{m_e \nu_{ij}} n_i f_{ij} \left(\frac{dv_r}{dr} \right)^{-1}, \quad (17)$$

where ν_{ij} is the line frequency, f_{ij} is the oscillator strength, and n_i, n_j are the number densities of individual states with statistical weights g_i, g_j . From this equation it follows that the effect of the resonance line scattering in the cool wind is effective mainly for stars with high mass-loss rates or for stars where X-rays more significantly influence the ionization equilibrium (i.e., stars with large f_X , where higher fractions of He-like ions emerge).

For stars HD 93204, 162978, 209975, and 210839 the resonance line scattering in the cool wind is able to influence the emergent X-ray line profiles of N VI and in some cases also of O VII (see Fig. 16). This effect, discussed also by Oskinova et al. (2006b), is sensitive to the properties of X-ray sources.

8 DISCUSSION

8.1 The dependence of f_X on the cooling time

The parameter f_X is an important free parameter that determines the wind X-ray luminosity. As it was used for some models, it is possible to specify f_X individually for each star using observed X-ray luminosity. As with fixed f_X we predict steeper $L_X - L$ relation than observed (Fig. 2), f_X which is inversely proportional to the luminosity would lead to a $L_X - L$ relation that better corresponds to the observed one.

The inverse proportionality of f_X on L (or on the wind density) may be a more realistic one. The total X-ray emissivity is given by the amount of energy dissipated by the shocks and the fraction of X-ray emitting material (or f_X) may be determined by this dissipated energy and by the cooling length. In fact, f_X may be lower for stars with dense winds in which the hot material is able to cool down

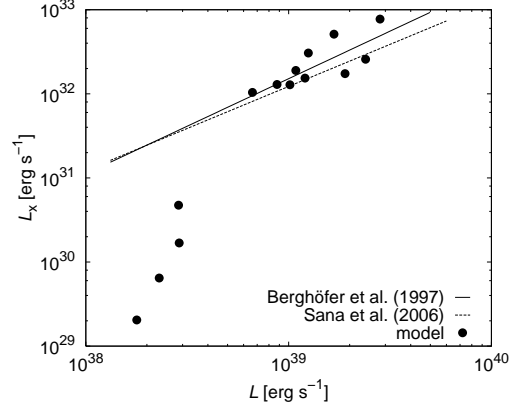


Figure 17. The X-ray luminosity calculated assuming the dependence of f_X on the cooling time via equation (18) in comparison with observations.

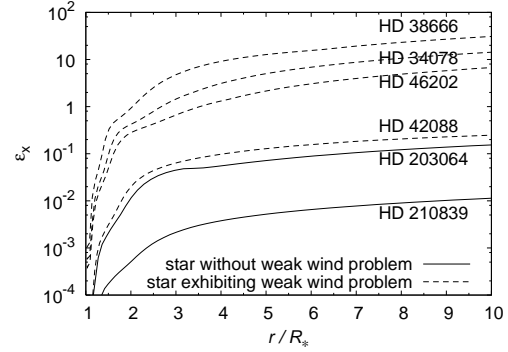


Figure 18. The radial variations of ϵ_X (see equation (18)) for selected stars.

more efficiently. To correct our results for the dependence of f_X on the cooling time, we calculated wind models where f_X is scaled by the value of the cooling time relatively to the hydrodynamical time-scale (cf. Antokhin et al. 2004; Zhekov & Palla 2007), i.e. roughly given by

$$f_X = f_0 \epsilon_X \equiv f_0 \frac{a_{\text{He}}^2 \rho}{(\xi \rho)^2 \int_0^\infty \Lambda(T_X) d\nu} \frac{v_r}{r}, \quad (18)$$

where we assume $f_0 = 0.7$. Since according to (18) $f_X \sim r$, L_X now increases ad infinitum. To avoid a possible divergence of L_X we limit f_X in (18) by a certain value, namely $f_X \leq 0.1$ as in the outer regions shocks may become adiabatic or weaker (Feldmeier et al. 1997a,b). The derived relation between L_X and L in Fig. 17 shows a good agreement with observations indicating that the variable cooling time may indeed be an important property of wind shocks.

8.2 The weak wind problem

Comparison of mass-loss rates derived from observation with the predicted ones (Table 3) shows that there is a good agreement between observation and theory for stars with large mass-loss rates $\dot{M} \gtrsim 10^{-7} M_\odot \text{ yr}^{-1}$ (provided that the observations are not significantly influenced by clumping). The situation is markedly different for stars with lower mass-loss rates $\dot{M} \lesssim 10^{-7} M_\odot \text{ yr}^{-1}$ (except HD 149757). The predicted mass-loss rates are generally by order of magnitude higher than those derived from observations.

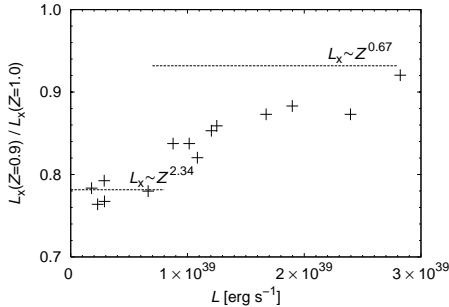


Figure 19. The ratio between the calculated X-ray fluxes from models with metallicities $Z = 0.9$ and $Z = 1$ (for the same $f_X = 0.02$). The dashed lines denote the approximate relations (equations (19), (20)).

These stars exhibit the so-called “weak wind problem”, whose solution is not yet known (Bouret et al. 2003; Martins et al. 2004, M05, Krtićka 2006).

The X-ray activity of these stars is higher than that of stars which do not exhibit the weak wind problem. Within our models this means that their X-ray luminosity predicted assuming a fixed filling factor is by two to three orders of magnitude lower than the observed one (see Fig. 2). However, the X-ray emission of these stars may still originate in the wind, because their X-ray luminosity is lower than the wind kinetic energy lost per unit of time $1/2\dot{M}v_\infty^2$ (M05). Note that due to low wind density of these stars the cooling length may become comparable with the hydrodynamical scale (as indicates the plot of ϵ_X in Fig. 18). Consequently, there is a possibility that once the wind of these stars is heated by the shocks it is not able to cool down sufficiently, and remains hot and unaffected by the radiative acceleration. This can be a reasonable explanation of the “weak wind problem” and high X-ray luminosity L_X of these stars. A similar scenario was invoked by Cohen et al. (2008) to explain the X-ray spectrum of β Cru.

8.3 The metallicity dependence

To discuss the influence of metallicity on L_X we recalculated our models with lower value of the mass fraction of heavier elements Z . Because the dependence of the free parameter f_X on metallicity is not known, we calculated these models with fixed f_X .

The derived variations of L_X with Z given in Fig. 19 can be easily interpreted. The mass-loss rate depends on metallicity roughly as $\dot{M} \sim Z^{0.67}$ (Krtićka 2006). The X-ray emission originates mainly from lines of heavier elements, thus we can assume that the emissivity per unit of mass depends on the metallicity roughly as $\Lambda_\nu(T_X) \sim Z$. Consequently, from the relations of OC (see Section 4.1) the optically thin X-ray luminosity scales with the metallicity as

$$L_X \sim Z^{2.34}. \quad (19)$$

In the optically thick case we can assume that for higher frequencies ($\nu \gtrsim 1 \times 10^{17}$ Hz) the X-ray opacity κ_X is mostly due to direct and inner-shell ionization of heavier elements. As a result of this $\kappa_X \sim Z$, and in the optically thick case the relations of OC yield $L_X \sim M\Lambda_\nu/\kappa_X$, i.e.

$$L_X \sim Z^{0.67}. \quad (20)$$

The relations (19) and (20) are derived assuming that f_X does not depend on the metallicity. However, lower value of Λ for lower metallicities could effectively mean that the cooling time of the gas

in the post-shock region is longer. Consequently, f_X may become higher for lower metallicities. In such a case we can expect the dependence of f_X on the metallicity roughly as $f_X \sim Z^{-1}$. Within this approximation the total X-ray luminosity would scale as

$$L_X \sim Z^{1.3} \quad (\text{optically thin case}), \quad (21a)$$

$$L_X \sim Z^{-0.3} \quad (\text{optically thick case}). \quad (21b)$$

8.4 Multicomponent effects

The multicomponent effects due to inefficient collisions between individual wind particle components may significantly influence structure of low-density winds (e.g., Springmann & Pauldrach 1992; Krtićka 2006). The Coulomb frictional force between wind components depends on the charge of these components, which may be influenced by the presence of X-rays. However, our tests showed that such influence is in most cases insignificant, because the X-rays typically modify the fraction of minor ionization stages only.

We tested whether the multicomponent effects are important for stars exhibiting the “weak-wind problem”. For this purpose we treated heavier elements as individual components (as in Krtićka 2006). We concluded that phosphorus due to its low abundance may decouple from the wind of HD 34078 and HD 38666, and the velocity difference between phosphorus and hydrogen is high also in the wind of HD 46202. For these stars the multicomponent effects and the ionization shift induced by it may be important.

8.5 Model simplifications

The inclusion of additional X-ray sources into our NLTE wind models was done assuming a simplified shock picture, in reality these sources may have slightly different properties. For example, the X-ray source can not be described just by one temperature (Feldmeier et al. 1997a). However, the main result of this paper, i.e., that the presence of X-rays does not significantly influence the wind parameters of O stars was justified for a broad range of shock parameters. On the other hand, the predicted ionization structure is much more sensitive to properties of X-ray sources.

There is a growing observational evidence that hot stars winds are clumped (Bouret et al. 2003; Martins et al. 2004; Puls et al. 2006b). We postpone the effect of clumping on the wind structure for a special study. The clumping may influence not only the comparison of ionization fractions derived from observation and from the theoretical models, but also modify the radiative force and the mass-loss rates (Krtićka et al. 2007; de Koter et al. 2007). On the other hand, the effect of porosity (Owocki et al. 2004; Oskinova et al. 2006a) may lead to decrease of the effective opacity in the X-ray region. This may affect the total X-ray luminosity, but as the porosity affects also the predicted wind parameters (Krtićka et al. 2007) and as its existence in the wind is a matter of discussion nowadays, we do not include it into our models. Note that the present approach of the inclusion of both clumping and porosity into wind models is based on *free* parameters whose values are not very well observationally nor theoretically constrained.

9 CONCLUSIONS

We studied an effect of additional X-ray emission on our NLTE wind models. To this end, we assumed that some part of the wind

material is heated to a very high temperature (of order of 10^6 K) and emits X-rays, and we studied their influence on wind structure.

Using our wind models we derived the same scaling of the total X-ray luminosity L_X with the mass-loss rate \dot{M} as Owocki & Cohen (1999). For stars with optically thick winds most of X-rays are absorbed in the wind, and the X-ray luminosity scales with wind mass-loss rate roughly as $L_X \sim \dot{M}$. For stars with optically thin wind in the X-ray region the X-ray luminosity scales as $L_X \sim \dot{M}^2$.

The models with fixed filling factor f_X can roughly explain the observed L_X/L relation of stars with optically thick wind in the X-ray region. The remaining deviation between the observed slope of the L_X/L relation and that derived using fixed f_X can be the result of the dependence of the shock cooling time on wind density. The stars with optically thin wind exhibiting the "weak wind problem" emit more X-rays than predicted by a simple optically thin scaling. Their enhanced X-ray emission and the "weak wind problem" itself may be caused by large wind shock cooling time, comparable with the hydrodynamical time scale.

The X-rays influence the ionization state in the whole wind. However, a significant amount of X-rays is emitted only in highly supersonic wind regions. These X-rays mostly do not penetrate close to the stellar surface, consequently the ionization changes induced by X-rays there are not large enough to change the radiative force there significantly. Because the mass-loss rate is determined in the region close to the stellar surface, the presence of X-rays does not significantly change its value. On the other hand, the terminal velocity is determined in the outer wind regions where the influence of X-rays is more important. Consequently, the wind terminal velocity may be slightly affected by X-rays, especially for stars with weaker ionizing continua (with $T_{\text{eff}} \lesssim 35\,000$ K).

Although the Auger processes are important for the ionization balance in the outer wind regions, the non-negligible presence of higher ionization stages (sometimes also called "superions") is a consequence of also a direct ionization.

We compared the model ionization fractions with those derived from observations. For higher ionization stages the inclusion of X-rays leads to better agreement between theory and observations. However, for many ions a significant discrepancy between theory and observations still remains. The discrepancy between the mass-loss rates derived from the $H\alpha$ line or radio emission and P V line profiles led Fullerton et al. (2006) to conclusion that real wind mass-loss rates of hot stars are much lower than the "classical" ones. This conclusion is sensitive to the assumed P V ionisation fraction. We have shown that for stars with $T_{\text{eff}} \gtrsim 34\,000$ K the P VI ion becomes a dominant one, which gives a better agreement for hotter stars. But even for these hotter stars a significant disagreement between theory and observations remains. We did not find any significant influence of X-rays on P V ionization fraction. Our calculations suggest that the effect of X-rays cannot be the reason the P V mass-loss rates are low. This problem is especially severe for stars with $T_{\text{eff}} \lesssim 34\,000$ K for which we predict P V to be the dominant ionization stage in the wind.

We studied the influence of modified ionization equilibrium due to shock emission on the X-ray line transfer. While continuum absorption by the cool wind in the X-ray domain is not significantly affected by X-rays itself, additional line opacity sources in a cool wind emerge (see also Oskinova et al. 2006b). This may affect the line profiles of more abundant elements (C, N, and O) observed in the X-ray spectra.

We can conclude that although the inclusion of X-rays into NLTE wind models leads to a better agreement between theory and

observation, it can not explain the most painful problems of present hot star wind research, i.e., lower mass-loss rates derived from observation with taking into account clumping, and too-low ionization fractions of P V derived from observations.

ACKNOWLEDGEMENTS

We thank to the anonymous referee for his/her comments that helped to improve the manuscript. We thank to Dr. J. Puls for the discussion and providing us atomic data, and to Prof. S. Owocki, Drs. L. Oskinova and V. Votruba for the discussion. This research has made use of NASA's Astrophysics Data System and the SIMBAD database, operated at CDS, Strasbourg, France. This work was supported by grant GA AV ČR B301630501, and later also by a grant GA ČR 205/08/0003.

APPENDIX A: CALCULATION OF DIAGONAL ELEMENTS OF Ψ_ν

The equation of the radiative transfer (13) is solved using the LU decomposition,

$$\Psi_\nu^{-1} = \mathbf{L}\mathbf{U}, \quad (\text{A1})$$

where \mathbf{L} is a product of permutation and lower triangular matrices with 1 subdiagonal, and \mathbf{U} is upper triangular matrix with 2 superdiagonals. In such a case the inversion matrix Ψ_ν can be easily calculated (Ralston 1965) as

$$\Psi_\nu = \mathbf{U}^{-1}\mathbf{L}^{-1}, \quad (\text{A2})$$

where \mathbf{U}^{-1} and \mathbf{L}^{-1} are upper and lower diagonal matrices. If we denote $\mathbf{u} \equiv \mathbf{U}^{-1}$ and

$$u_{i,i} = U_{i,i}^{-1}, \quad (\text{A3})$$

$$u_{i,j} = -\frac{u_{i,j-1}U_{j-1,j} + u_{i,j-2}U_{j-2,j}}{U_{j,j}}, \quad (\text{A4})$$

and similarly for \mathbf{L}^{-1} . From this, diagonal elements of Ψ_ν can be easily calculated.

Instead of using matrix inversion it is possible to derivate (13) with respect to the occupation number N_i and calculate partial derivatives $\partial J_\nu / \partial N_j$ as a solution of derived system of linear equations. Although this would be likely fast solution (remember that since we employ LU decomposition for the solution of equation 13, we can use this solution procedure to solve other equations with the same matrix), we would have to solve these equations for each N_j , and this would be very time consuming.

REFERENCES

- Anderson E. et al., 1999, LAPACK Users' Guide, 3rd ed., SIAM, Philadelphia
- Asplund M., Grevesse N., Sauval A. J., 2005, in T. G. Barnes III, F. N. Bash, eds., ASP Conf. Ser. 336, Cosmic Abundances as Records of Stellar Evolution and Nucleosynthesis, Astron. Soc. Pac., San Francisco, p. 25
- Antokhin I. I., Owocki S. P., Brown J. C., 2004, ApJ, 611, 434
- Auer L. H., 1971, JQSRT, 11, 573
- Auer, L. H. 1987, in Numerical Radiative Transfer, W. Kalkofen ed., Cambridge Univ. Press, p. 101
- Babel J., Montmerle T., 1997, A&A, 323, 121

- Bautista M. A., 1996, *A&AS* 119, 105
- Bautista M. A., Pradhan A. K., 1997, *A&AS* 126, 365
- Berghöfer T. W., Schmitt J. H. M. M., Cassinelli J. P., 1996, *A&AS*, 118, 481 (BSC)
- Berghöfer T. W., Schmitt J. H. M. M., Danner R., Cassinelli J. P., 1997, *A&A*, 322, 167
- Bouret J.-C., Lanz T., Hillier D. J., Heap S. R., Hubeny I., Lennon D. J., Smith L. J., Evans C. J., 2003, *ApJ*, 595, 1182
- Butler K., Mendoza C., Zeippen C. J., 1993, *J. Phys. B* 26, 4409
- Cassinelli J. P., Olson G. L., 1979, *ApJ*, 229, 304
- Castor J. I., 1974, *MNRAS*, 169, 279
- Castor J. I., Abbott D. C., Klein R. I., 1975, *ApJ*, 195, 157 (CAK)
- Chen G. X., Pradhan A. K., 1999, *A&AS*, 136, 395
- Chlebowski T., Garmany C. D., 1991, *ApJ*, 368, 241
- Chlebowski T., Harnden F. R., Sciortino S., 1990, *ApJ*, 341, 427
- Cohen D. H., Kuhn M. A., Gagné M., Jensen E. L. N., Miller N. A., 2008, *MNRAS*, 386, 1855
- de Koter A., Vink J. S., Muijres L., 2007, in Hamann W.-R., Feldmeier A., Oskinova L., eds, *Clumping in Hot Star Winds*, 47
- Evans N. R., Seward F. D., Krauss M. I., Isobe T., Nichols J., Schlegel E. M., Wolk S. J., 2003, *ApJ*, 589, 509
- Fernley J. A., Taylor K. T., Seaton, M. J., 1987, *J. Phys. B*, 20, 6457
- Feldmeier A., Kudritzki R.-P., Palsa R., Pauldrach, A. W. A., Puls J., 1997a, *A&A*, 320, 899
- Feldmeier A., Puls J., Pauldrach, A. W. A., 1997b, *A&A*, 322, 878
- Feldmeier A., Oskinova L., Hamann W.-R., 2003, *A&A*, 403, 217
- Fullerton A. W., Massa D. L., Prinja R. K., 2006, *ApJ*, 637, 1025
- Hempe K., Schönberg K., 1986, *A&A*, 160, 141
- Herrero A., Kudritzki R. P., Vilchez J. M., Kunze D., Butler K., Haser, S., 1992, *A&A*, 261, 209
- Howarth I. D., Prinja R. K., 1989, *ApJS*, 69, 527
- Hubeny I., 1988, *Comput. Phys. Commun.* 52, 103
- Hubeny I., 2003, I. Hubeny, D. Mihalas & K. Werner eds., in *Stellar Atmosphere Modelling*, ASP Conf. Ser., Vol. 288, 17
- Hubeny I., Lanz T., 1992, *A&A* 262, 501
- Hubeny I., Lanz T., 1995, *ApJ* 439, 875
- Hummer D. G., Berrington K. A., Eissner W., Pradhan A. K., Saraph H. E., Tully, J. A., 1993, *A&A*, 279, 298
- Ignace R., Gayley K. G. 2002, *ApJ*, 568, 954
- Kaastra J. S., Mewe R., 1993, *A&AS*, 97, 443
- Kahn S. M., Leutenegger M. A., Cottam, J., Rauw G., Vreux J.-M., den Boggende A. J. F., Mewe R., Güdel M., 2001, *A&A*, 365, L312
- Krtićka J., 2006, *MNRAS*, 367, 1282
- Krtićka J., Kubát J., 2004, *A&A*, 417, 1003 (Paper I)
- Krtićka J., Kubát J., 2007, *A&A*, 464, L17
- Krtićka J., Puls J., Kubát J., 2007, in Hamann W.-R., Feldmeier A., Oskinova L., eds, *Clumping in Hot Star Winds*, 111
- Kubát J., 1993, PhD thesis, *Astronomický ústav AV ČR, Ondřejov*
- Kubát J., Puls J., Pauldrach A. W. A., 1999, *A&A* 341, 587
- Kubát J., Krtićka J., Pustyl'nik, I., 2004, *New Astronomy*, 9, 215
- Kudritzki R. P., Puls J., 2000, *ARA&A*, 38, 613
- Kupka F., Piskunov N. E., Ryabchikova T. A., Stempels H. C., Weiss W. W., 1999, *A&AS* 138, 119
- Lamers H. J. G. L. M., Leitherer C., 1993, *ApJ* 412, 771
- Lamers H. J. G. L. M., Haser S., de Koter A., Leitherer C., 1999, *ApJ*, 516, 872
- Lamers H. J. G. L. M., Snow T. P., Lindholm D. M., 1995, *ApJ*, 455, 269 (LSL)
- Lanz T., Hubeny I., 2003, *ApJS*, 146, 417
- Leutenegger M. A., Paerels F. B. S., Kahn, S. M., Cohen D. H., 2006, *ApJ*, 650, 1096
- Leutenegger M. A., Owocki S. P., Kahn S. M., Paerels F. B. S., 2007, *ApJ*, 659, 642
- Luo D., Pradhan A. K., 1989, *J. Phys. B*, 22, 3377
- MacFarlane J. J., Cohen D. H., Wang P., 1994, *ApJ*, 437, 351
- Markova N., Puls J., Repolust, T., Markov, H., 2004, *A&A*, 413, 693 (M04)
- Martins F., Schaerer D., Hillier D. J., Heydari-Malayeri M., 2004, *A&A*, 420, 1087
- Martins F., Schaerer D., Hillier D. J., Meynadier F., Heydari-Malayeri M., Walborn N. R., 2005, *A&A*, 441, 735 (M05)
- Massa D., Fullerton A. W., Sonneborn, G., Hutchings J. B., 2003, *ApJ*, 586, 996
- Mihalas D., 1978, *Stellar Atmospheres*, 2nd ed., W. H. Freeman & Co., San Francisco
- Mihalas D., Hummer D. G., 1974, *ApJS*, 28, 343
- Miller N. A., Cassinelli J. P., Waldron W. L., MacFarlane J. J., Cohen D. H., 2002, *ApJ*, 577, 951
- Nahar S. N., Pradhan A. K., 1993, *J. Phys. B* 26, 1109
- Nahar S. N., Pradhan A. K., 1996, *A&AS* 119, 509
- Ng K. C., 1974, *J. Chem. Phys.*, 61, 2680
- Olson G. L., Castor J. I., 1981, *ApJ*, 244, 179
- Oskinova L. M., Feldmeier A., Hamann, W.-R., 2006a, *MNRAS* 372, 313
- Oskinova L. M., Hamann W.-R., Feldmeier A., 2006b, in G. Branduardi-Raymont, ed., *High Resolution X-ray Spectroscopy*, 27
- Oskinova L. M., Hamann W.-R., A. Feldmeier, 2007, *A&A*, 476, 1331
- Owocki S. P., Cohen D. H., 1999, *ApJ*, 520, 833 (OC)
- Owocki S. P., Cohen D. H., 2001, *ApJ*, 559, 1108
- Owocki S. P., Cohen D. H., 2006, *ApJ*, 648, 565
- Owocki S. P., Castor J. I., Rybicki G. B., 1988, *ApJ*, 335, 914
- Owocki S. P., Gayley K. G., Shaviv N. J., 2004, *ApJ*, 616, 525
- Pauldrach A. W. A., 1987, *A&A*, 183, 295
- Pauldrach A. W. A., Kudritzki R. P., Puls, J., Butler K., Hunsinger J., 1994, *A&A*, 283, 525
- Pauldrach A. W. A., Hoffmann T. L., Lennon, M., 2001, *A&A*, 375, 161
- Piskunov N. E., Kupka F., Ryabchikova T. A., Weiss, W. W., Jeffery C. S., 1995, *A&AS*, 112, 525
- Prilutskii O. F., Usov V. V., 1976, *AZh*, 53, 6
- Puls J., Kudritzki R.-P., Herrero A., Pauldrach A. W. A., Haser S. M. et al., 1996, *A&A* 305, 171
- Puls J., Repolust T., Hoffmann T., Jokuthy A., Venero R. O. J., 2003, in K. A. van der Hucht, A. Herrero, C. Esteban, eds., *A Massive Star Odyssey: From Main Sequence to Supernova*, IAU Symp 212, ASP, p. 61
- Puls J., Markova N., Scuderi S., 2006a, in A. de Koter, L. Smith, R. Waters, eds., *Mass loss from stars and the evolution of stellar clusters*, in press (astro-ph/0607290)
- Puls J., Markova N., Scuderi S., Stanghellini C., Taranova O. G., Burnley A. W., Howarth I. D., 2006b, *A&A*, 454, 625 (P06)
- Raassen A. J. J., Cassinelli J. P., Miller N. A., Mewe R., Tepedelenliolu E., 2005, *A&A*, 437, 599
- Ralston A., 1965, *A first course in numerical analysis*, McGraw-Hill, New York
- Raymond J. C., 1988, in R. Pallavicini ed., *Hot Thin Plasmas in Astrophysics*, NATO ASI Series C, Volume 249, p. 3
- Raymond J. C., Smith B. W., 1977, *ApJS*, 35, 419
- Repolust T., Puls J., Herrero A., 2004, *A&A*, 415, 349 (R04)

- Runacres M. C., Owocki S. P., 2002, *A&A* 381, 1015
Rybicki G. B., Hummer D. G., 1992, *A&A*, 262, 209
Sana H., Rauw G., Naz Y., Gosset E., Vreux J.-M., 2006, *MNRAS*, 372, 661
Sawey P. M. J., Berrington K. A., 1992, *J. Phys. B*, 25, 1451
Schaller G., Schaerer D., Meynet G., Maeder A., 1992, *A&AS*, 96, 269
Seaton M. J., 1987, *J. Phys. B*, 20, 6363
Seaton M. J., Zeippen C. J., Tully J. A., Pradhan A. K., Mendoza C., Hibbert A., Berrington K. A., 1992, *Rev. Mexicana Astron. Astrofis.*, 23, 19
Springmann U. W. E., Pauldrach A. W. A. 1992, *A&A*, 262, 515
ud-Doula A., Owocki S. P., 2002, *ApJ*, 576, 413
Verner D. A., Yakovlev D. G., 1995, *A&AS*, 109, 125
Verner D. A., Yakovlev D. G., Band I. M., & Trzhaskovskaya M. B., 1993, *Atomic Data and Nuclear Data Tables*, 55, 233
Vink J. S., de Koter A., & Lamers H. J. G. L. M., 2000, *A&A* 362, 295
Waldron W. L., Cassinelli J. P., 2007, *ApJ*, 668, 456
Zhang H. L., 1996, *A&AS*, 119, 523
Zhang H. L., Pradhan A. K., 1997, *A&AS*, 126, 373
Zhekov S. A., Palla F., 2007, *MNRAS*, 382, 1124